Application of an electrostatic machine in a low-voltage micro-grid

Gabriel Ramos Huerta, Patricio Mendoza-Araya
UNIVERSITY OF CHILE
Energy Center, Electrical Engineering Department
Av. Tupper 2007, Santiago, Chile
Phone: +56 (2) 2978 4768
Email: gabriel.ramos.h@ug.uchile.cl, pmendoza@ing.uchile.cl

Keywords

≪Electrical machines≫, ≪Microgrid≫, ≪Synchronous motor≫, ≪Stability≫, ≪Fault tolerance≫.

Acknowledgments

The authors would like to thank the the Electrical Engineering Department and the Energy Center of the University of Chile for the financial aid.

Abstract

In this work, dq axis models and equations for an electrostatic machine (ESM) are implemented. Speed and excitation controllers are adapted for this machine, and tests are run to check their performance. Finally, this machine is inserted into a micro-grid environment (CIGRE low voltage benchmark micro-grid) to find its possible contributions to the system regulation and short circuit currents.

Introduction

Back in the 1830's decade, Michael Faraday discovered what would become one of the most important laws in electromagnetism: the *Electromagnetic Induction* law. Later, this discovery would lead the scientific communities to study and model one of the most recognized kind of machines: the electromagnetic machine (EMM). This machine, thanks to its sturdiness, efficiency and stability, would then become the protagonist of electrical power systems.

At the same time, Jean Peltier was making another big discovery: the *Electrostatic Induction* law. Though, his discovery would pass rather unnoticed until the 1920's, when Van de Graaff created his famous electrostatic machine (ESM) named after him. This machine was rather inefficient and hard to build; and since electromagnetic machines had taken over the electrical systems, they were left aside.

No theoretical basis for the ESM would be developed until 1960's, when Dominique Gignoux [1], along with F. J. McCoy and W. R. Bell [2] revisited it. They concluded that this machine's principle of work was, as a generation method, inefficient; but it could eventually work if there were any kind of fluid development that would tolerate the existence of strong electric fields with no electric arcs, i.e. strong dielectrics.

Recently, dielectric fluid development has reached new goals [3]. This encouraged the study of the ESM as an energy generation method. Mainly, two relevant works have been made [4] [5]; in these, electrostatic motor prototypes are built, considering a strong mathematical modelling. These prototypes feature a high amount of poles, lack of iron core, small power capacity and the use of a dielectric fluid in order to avoid electrical discharges.

Most of the recent research has been focused on the application of this machine as a motor. However, its application as a generator is appealing, particularly in a microgrid, considering the size of current

prototypes [4]. Given this machine's characteristics, which behaves in steady state as a current source, its incorporation as a generator might not be as usual. In this line, the main goal of this work is to explore and show what are the extents of this machine's benefits in a micro-grid environment, working as a generator.

The rest of the document is structured as follows. First, the main characteristics and equations of this machine will be provided; these will be then implemented using PLECS. Classical controller models will be adapted and implemented, in order to give this machine some sort of regulation. Finally, this machine will be inserted into CIGRE low voltage benchmark micro-grid, in order to evaluate its dynamic behavior. Finally, this work concludes giving some insight about this machine's properties, benefits and challenges.

Electrostatic Machine Modelling

As opposed to the conventional electromagnetic machine, this machine works with the electrostatic field induction principle. This means, instead of using an electromagnetic field to induce current, an electrostatic field is created to induce voltage. In order to reach a meaningful electrostatic field magnitude, high voltages are usually required.

A great work in ESM modeling and designing is provided in [4], where a small prototype was built. For the purposes of this paper, the most relevant equations and models are extracted and analyzed from [4], while the complete mathematical derivation of such models can be found in the cited reference.

dq axis models

The dq axis models for an ESM are presented in Figs. 1a and 1b (extracted from [4]), and the dq axis models for an electromagnetic machine are shown in Figs. 2a and 2b (extracted from [6]). These models do not include dampers:

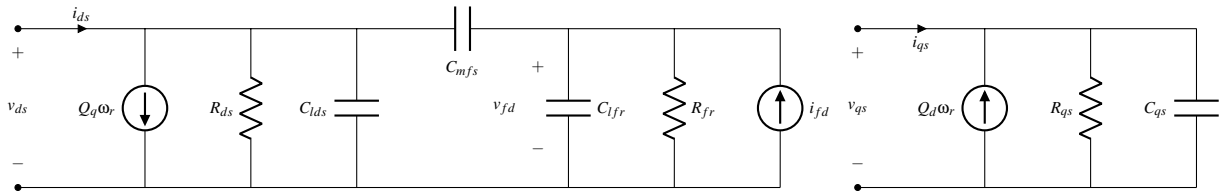

(a) d axis circuit (ESM)

(b) q axis circuit (ESM)

Fig. 1: dq axis for ESMs, no dampers

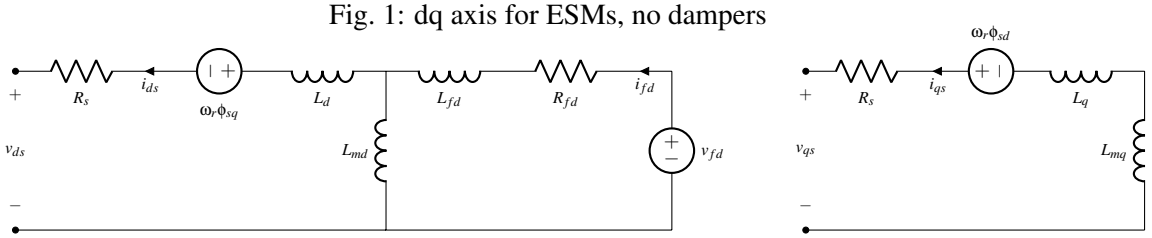

(a) d axis circuit (EMM)

(b) q axis circuit (EMM)

Fig. 2: dq axis for electromagnetic machines, no dampers

Table I: Subscript list

Subscript	Meaning
f	Field quantity
r	Rotor quantity
s	Stator quantity
d,q	d or q axis quantity
m	Stator - Rotor (mutual) quantity
l	Leakage quantity

The meaning of the subscript in Figs. 1 and 2 are listed in Table I. These show a duality between the electromagnetic and electrostatic machines:

- The existence of a *speed current* in the ESM, as a dual of the well known *speed voltage* present in electromagnetic machines, due to Park's transform.
- The presence of a key element that couples the rotor and stator circuits, represented as a mutual inductance in the electromagnetic machine. In the ESM, this element is depicted as a mutual capacitance C_{mfs}.
- In general, the ESM's dq circuits are shaped as the Norton's equivalent circuit of the electromagnetic's, although series RL circuits are replaced by parallel RC circuits.

Although the full model for the ESM can be readily obtained from the equivalent circuit in Fig. 1, only the most relevant equations are presented below. The output current of the machine I_{out} is

$$I_{out} = V_{fd} \cdot \omega_r \cdot C_m \tag{1}$$

where V_{fd} is the excitation voltage, ω_r is the angular frequency of the machine and C_m is the stator-rotor mutual capacitance. This equation shows the lineal dependence of the output current to the machine frequency.

The electrical power and torque provided by this machine are:

$$P_e = \frac{3}{2} \cdot (v^r_{ds} i^r_{ds} + v^r_{qs} i^r_{qs}) + 3 v_{fr} i'_{fr} \tag{2}$$

$$T_e = \frac{3P}{2} \cdot (C_m v^r_{qs} v_{fr}) \tag{3}$$

where P stands for the pole number. Also, the following capacitance values must be defined:

$$C_{lds} = C_{ds} - C_{mfs} \tag{4}$$

$$C_{lfr} = C_{fr} - C_{mfs} \tag{5}$$

where C_{ds} can be approximated by C_s for a cylindrical shape, hence $C_{mfs} = C_m$; these values will be later extracted from the short and open circuit tests performed in [4]. Finally, this machine is, like any other synchronous machine, subject to the Swing equation:

$$J \cdot \frac{d^2\theta_m}{d\theta^2} = T_m - T_e \tag{6}$$

where θ_m is the mechanical angle of the rotor, T_m, T_e are the mechanical and electrical torque and J is the machine inertia.

Metodology

In order to evaluate the ESM's dynamic behavior, the following methodology is proposed.

First, the machine is modeled in a simulation environment. Both dq axis circuits and relevant equations are implemented using PLECS software. In order to validate the machine implementation, short-circuit and open-circuit experiment results reported in [4] will be reproduced. It must be noted that dampers won't be modelled, as there is a lack of information about their electrical parameters.

After the validation, the CIGRE low-voltage benchmark micro-grid is modelled (Fig. 3). Since the original machine prototype built in [4] does not meet the power level required to participate in this micro-grid (tens of [kW]), a per-unit scaled model of the prototype is used. Then, this machine is introduced at the end of the residential feeder of the micro-grid, replacing the fuel cells (modelled as current source inverters).

In order to participate in the primary control of the system, classical controllers will be adapted for this machine; these consider an excitation controller and a speed controller. After their implementation, three tests are performed: load step, line disconnection and three-phase to ground short-circuit. Finally, the results are analyzed in an attempt to discover this machine's possible contributions to a micro-grid's transient response.

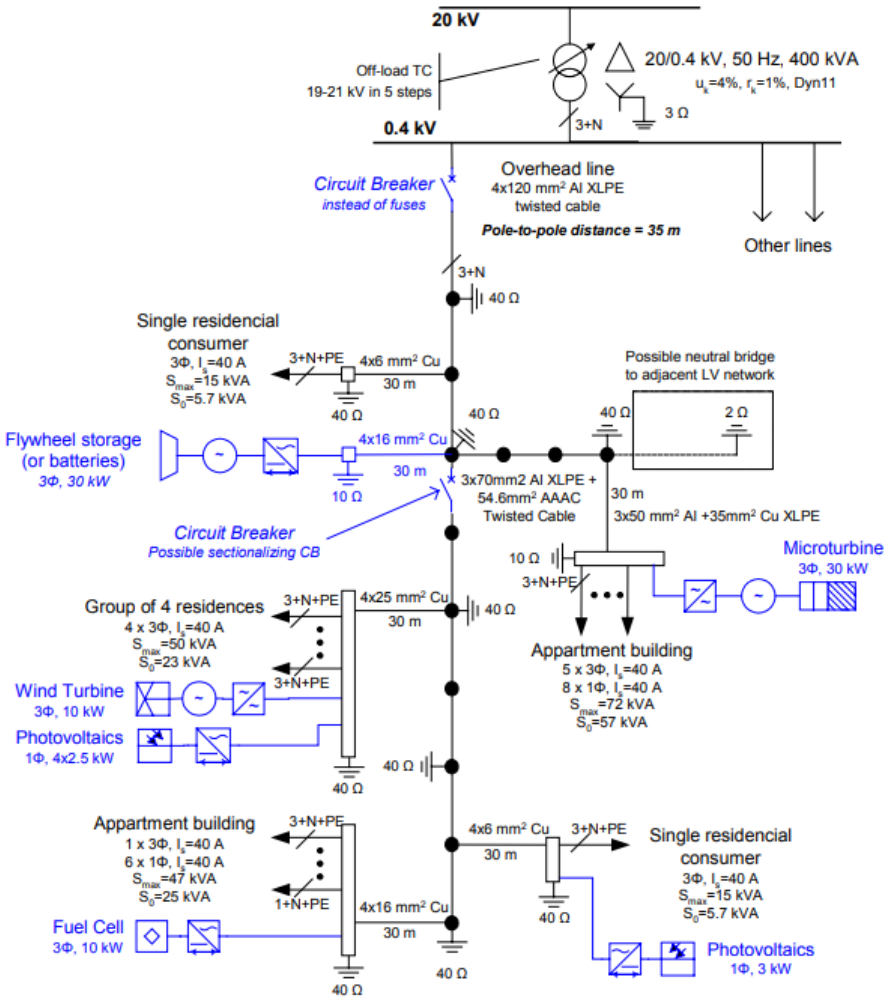

Fig. 3: CIGRE low voltage microgrid ([7])

Study Cases

The original CIGRE micro-grid (with the fuel cell) will be addressed as Case A. The case where this fuel cell is replaced with an ESM will be called Case B. On both setups, three experiments will be performed:

- Load step: a load increase of 40% is applied to the fuel cell / machine's busbar. This includes an increase in both active and reactive power consumption. The main goal of this experiment is to check the machine's primary control response, and the dynamic behavior during the system stabilization.
- Line disconnection: in this experiment, the line that connects both the residential consumer and the photovoltaics is disconnected via a breaker in the $4x6mm^2Cu,\ 30\ [m]$ line. The goal of this experiment is to provide insight on possible coordination's modifications on the protection scheme of the micro-grid.
- Short-circuit: the last experiment applies a three-phase short circuit with a small ground impendance. The objective is to detect the machine's contribution to short circuit currents.

Results

Machine model validation

The prototype machine parameters are listed in table II.

Table II: Parameters of the implemented electrostatic machine model

Parameter	Description	Value	Unit
C_f	Rotor capacitance	13.8	nF
C_m	Rotor-Stator capacitance	2.0	nF
C_s	Stator capacitance	13.8	nF
R_f	Rotor resistance	50	$M\Omega$
R_s	Stator resistance	1.7	$M\Omega$
p	Pole number	96	-

The results of performing the short and open circuit tests are shown in figures 4a and 4b.

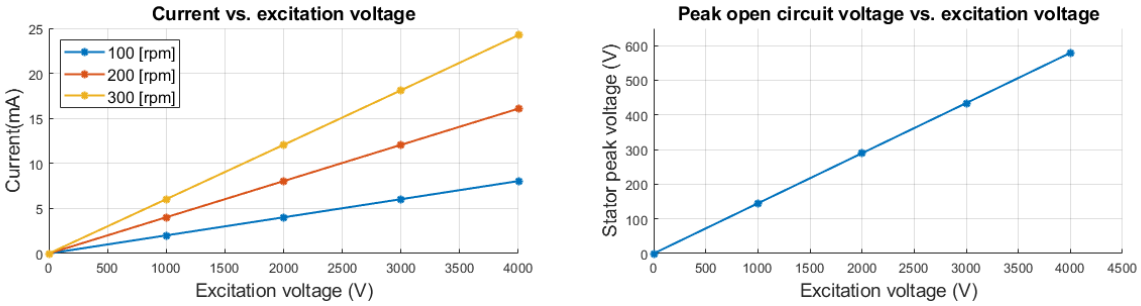

(a) Short circuit test

(b) Open circuit test

Fig. 4: Results for short and open circuit tests

These results closely match the ones obtained in [4], during the practical tests of the machine. Hence, the electrostatic machine model in the simulation environment is successfully verified.

Re-sizing of the machine

Since this machine's nominal values are not an adequate fit for the power levels required by the CIGRE microgrid, a resizing is performed using the electrical parameters provided by [4] and CIGRE's nominal voltage and a chosen power capacity. New impedances are rescaled by the following factor:

$$Z_{re-scaled} = Z_{original} \cdot \frac{Z_{base}^{new}}{Z_{base}^{old}} \tag{7}$$

Where Z_{base}^{new} and Z_{base}^{old} are calculated with the nominal parameters:

$$Z_{base}^{new} = \frac{(230 \cdot \sqrt{2})^2}{15000} \tag{8}$$

$$Z_{base}^{old} = \frac{3500^2}{300} \tag{9}$$

where $Z = V^2/S$ was used. The power value for the prototype (300 [W]) was never explicitly listed, but described as *fraction of a horsepower* in [5]. Also, the pole number of the machine is reduced to 30, in order to keep the machine working at a reasonable speed (100 rpm, as mentioned in [4]).

To estimate this machine's inertia, a small diesel generator is considered as reference [8]. Since the electromagnetic's machine inertia considers an iron core and this machine is of a smaller capacity (12.5 [kW]), an estimated value of 2 [kgm^2] is used.

Controllers

A DC2A AVR is adapted for current control (ACR from now on, as in *Automatic Current Controller*), along with a DEGOV1 governor for speed control. DEGOV1 features no modifications; DC2A presents a slight modification in its reference input. Since this machine must be able to adapt to the requirements of the system, its output current cannot be a fixed value. A dynamic reference current is calculated using a power factor as a reference:

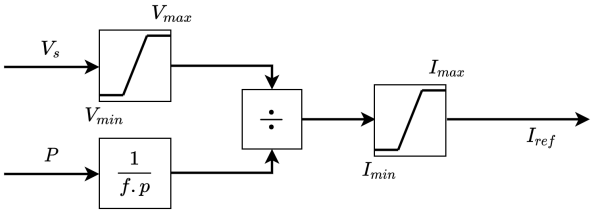

Fig. 5: Reference generation diagram for the ACR

In Fig. 5, the output active power of the machine is used to calculate a value for the apparent power S, using a power factor $f.p$. This, along with the measured voltage on the machine's point of connection, allows for a dynamic reference current calculation. Saturators are in place in order to ensure well defined divisions and reasonable reference current limits. The rest of the original AVR model remains the same.

The controllers' parameters are listed in table III; these were obtained from the range values listed in [9] and [10], respectively.

Table III: Values for adapted DC2A and DEGOV1

ACR		
Parameter	Value	Unit
TR	0.02	s
KA	150	p.u
KE	0.3	p.u
KF	0.3	p.u
TA	0.02	s
TB	0.02	s
TC	0.1	s
TE	1	s
TF	0.05	s
IMax	1.2	p.u
IMin	0.7	p.u
f.p	0.8	-

Governor		
Parameter	Value	Unit
K	12	p.u
T1	0.8	s
T2	0.1	s
T3	0.5	s
T4	0.16	s
T5	0.25	s
T6	0.01	s
TD	0.01	s
TMax	-0.5	p.u
TMin	1.5	p.u

CIGRE microgrid experiments

As described in the methodology, three experiments on the CIGRE microgrid are performed. The base values used for this microgrid are listed in table IV. Nominal values for the converters and its controllers are shown in table V and VI.

Table IV: Base values for CIGRE low voltage micro-grid

Parameter	Nominal value	Unit
Base rms voltage (single phase)	230	V
Base rms current (single phase)	21.739	A
Base power (three phase)	15000	W

Table V: Nominal parameters: CIGRE microgrid

Unit	Operating Mode	Active power [kW]	Reactive power [kVAr]
Microturbines	Grid Forming (VSI)	45	20
PV	Grid Following	3	1.5
Wind Turbines	Grid Following	10	5
Batteries	Grid Following	30	15
Fuel cell	Grid Forming (CSI)	15	8

Table VI: Inner and outer loop control values for CIGRE microgrid unit

Unit	Voltage loop		Current loop		Droop control	
	Kp	Ki	Kp	Ki	Mp (%)	Mq (%)
Microturbines	3	10	0.8	3	5	3
PV	-	-	0.9	0.8	-	-
Wind turbines	-	-	0.7	0.6	-	-
Batteries	-	-	0.5	0.6	-	-
Fuel cell	-	-	-	-	5	3

Load step

The results of applying a load increase of 40% in the apartment building load that shares busbar with the fuel cell are shown in Fig. 6. In that figure, the transient responses of both the fuel cell and the electrostatic machine (named "study unit") during the application of the load step is shown. Since the fuel cell droop control and the implemented ACR are fundamentally different, the steady state values are different; this is noticeable in Fig. 6b and 6d.

Fig. 6a shows the different frequency responses of the study units. It is clear that case B has a slower response, mainly due to the machine's inertia. This inertia is also noticeable in Figs. 6b and 6d; since this machine's output current varies linearly with the machine's frequency, the oscillations are even more evident in the output current response (6e).

Fig. 6c shows the amount of active power delivered by the study units. Just like the frequency response, it is rather slow, taking up to 4 [s] to reach a steady state value. During this transient, there must be another unit dispatching the required active power; in this case, it is the converter of the microturbines, operating in grid forming mode (Fig. 6f).

Since this machine operates as a current source, its transient response does not directly affect the system's voltage. The oscillations seen in Fig. 7 suggest that the machine's inertial response only affects the local busbar's voltage and the machine's output current frequency, and does not have a direct impact on the microturbines' output voltage frequency. All of these frequencies do eventually reach the same point, with damped oscillations that converge to the fundamental frequency component, determined by the microturbine's droop control. This may suggest that, the closer an electrostatic machine is to a voltage controlled inverter, the more impact it will have on the grid's voltage frequency.

This experiment proves that, even with classical controllers, this machine is able to participate in the grid's primary frequency control, although this controller does not allow for primary voltage control. The adapted controller, nevertheless, allows for a constant output power factor.

Line disconnection

The results for a line disconnection are shown in Fig. 8.

The main goal of this experiment is to detect similarities and differences between waveform responses during a fast-paced perturbation. It can be seen in Figs. 8c and 8d that the responses are very similar, and none of the currents feature high peaks. This suggests that, compared to a current controlled inverter, protection systems in the microgrid would not need to be tuned again, as the response of the machine is highly damped and of low amplitude. The peaks seen in Figs. 8a and 8b belong to that small window of time where the rms value, calculated with a very high sampling time, does vary due to the current peaks seen in the waveform figures.

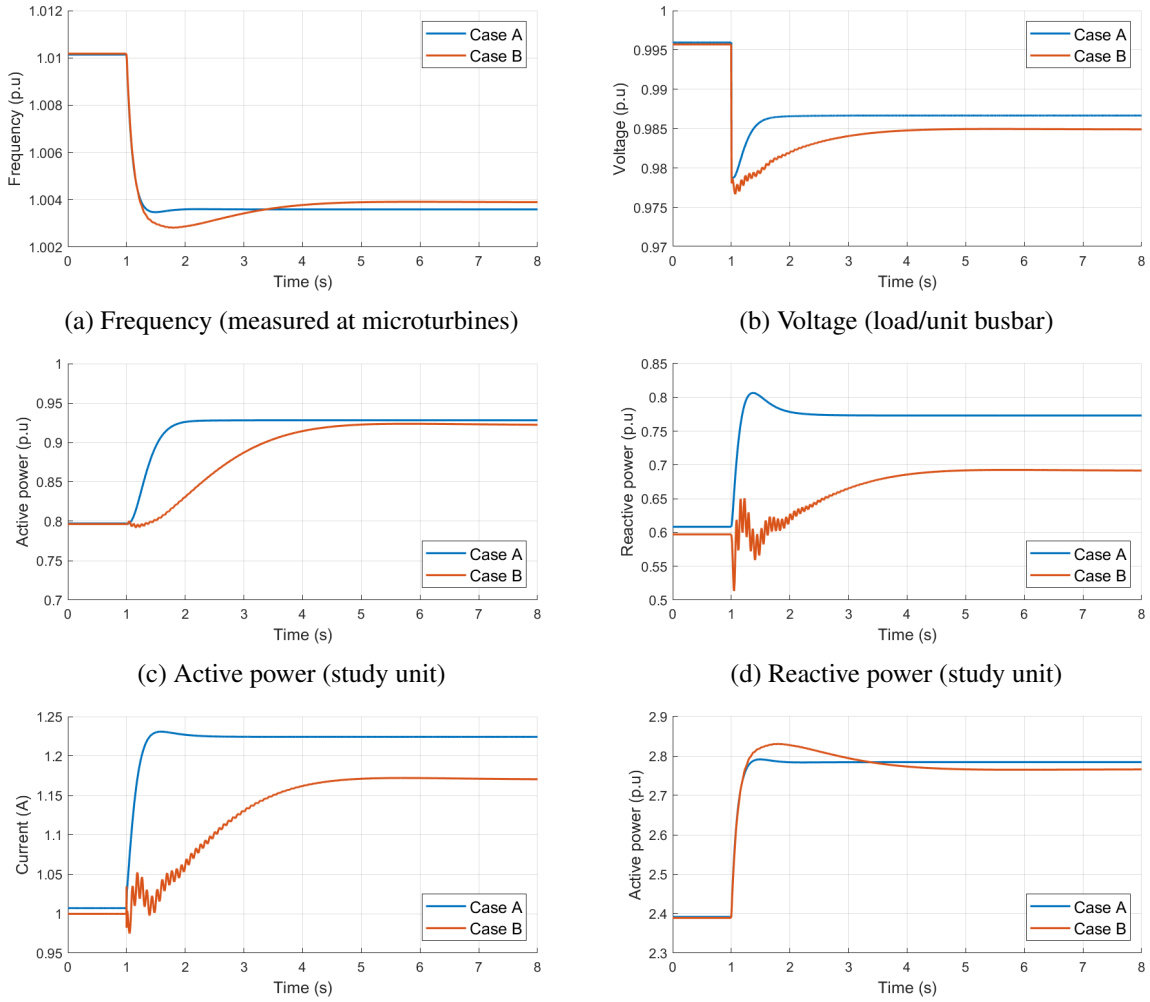

(a) Frequency (measured at microturbines)

(b) Voltage (load/unit busbar)

(c) Active power (study unit)

(d) Reactive power (study unit)

(e) Output current (study unit)

(f) Active power (microturbines)

Fig. 6: Results: load step

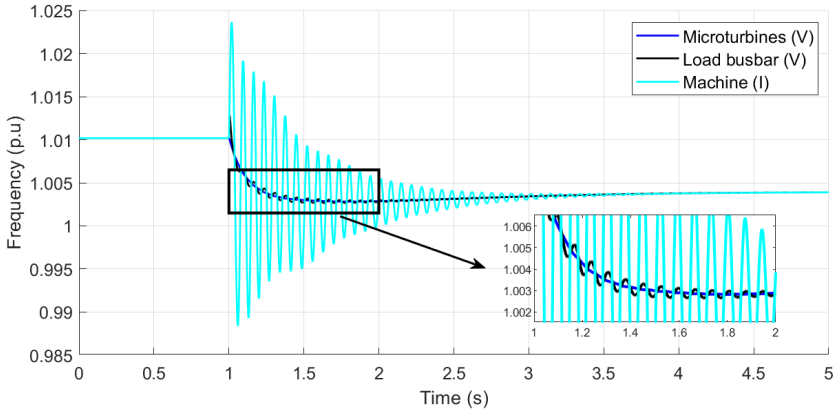

Fig. 7: Frequencies in the grid during the load step (V: frequency of voltage measurement, I: frequency of current measurement)

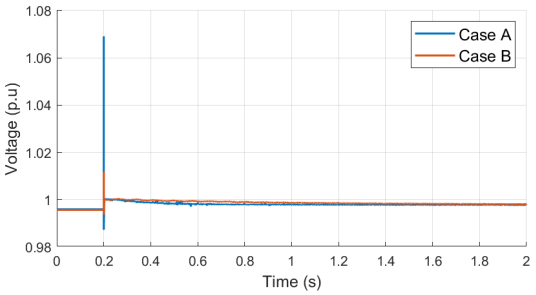

(a) Voltage (unit busbar)

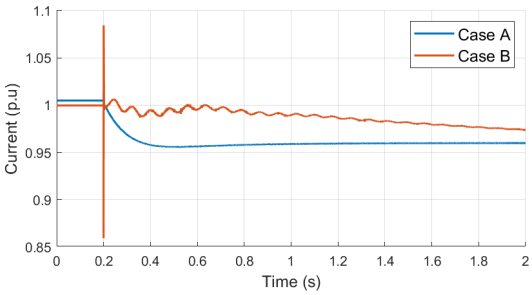

(b) Current (study unit)

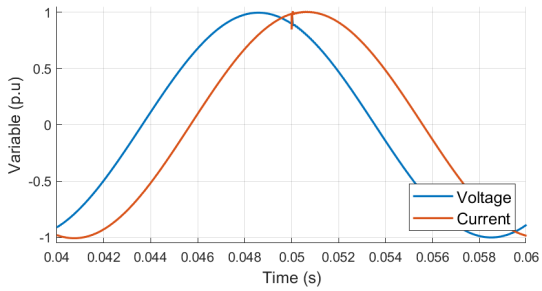

(c) Waveforms (fuel cell)

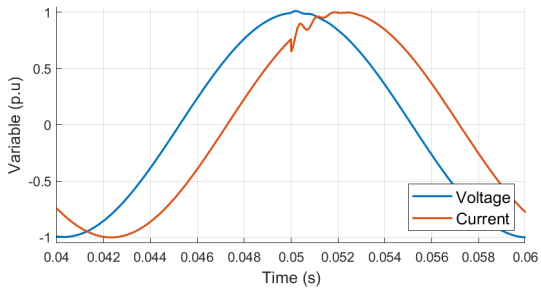

(d) Waveforms (ESM)

Fig. 8: Results: line disconnection

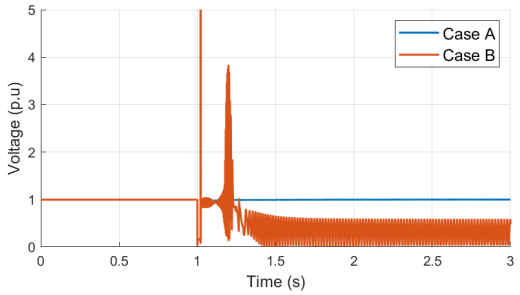

(a) Voltage (unit busbar)

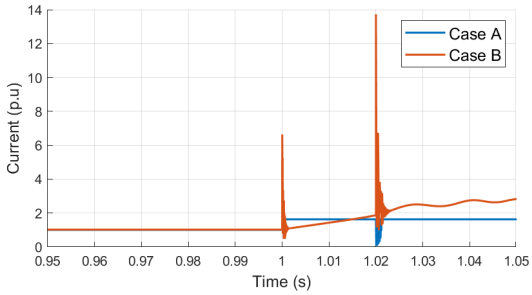

(b) Current (study unit)

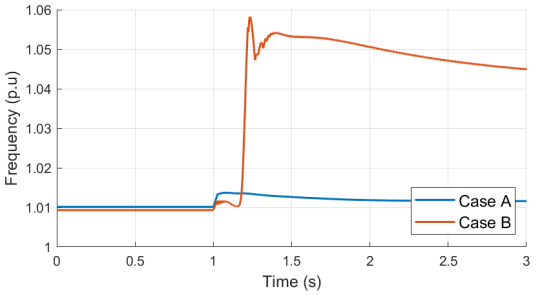

(c) Frequency (microturbines)

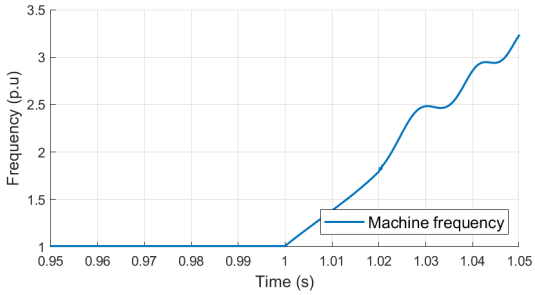

(d) Frequency (machine)

Fig. 9: Results: short circuit

Short circuit

The results of applying a short circuit at time 1 [s], and clearing it after 20 [ms], are shown in Fig. 9. These results show that the system is unstable for the case B. The electrostatic machine is unable to evacuate its input mechanical torque (shown separately in Fig. 10); this happens because, due to the sudden voltage drop, the amount of electrical torque perceived by the machine drops as well, in accordance to (3). The governor is unable to react as fast, causing the machine to drastically increase its

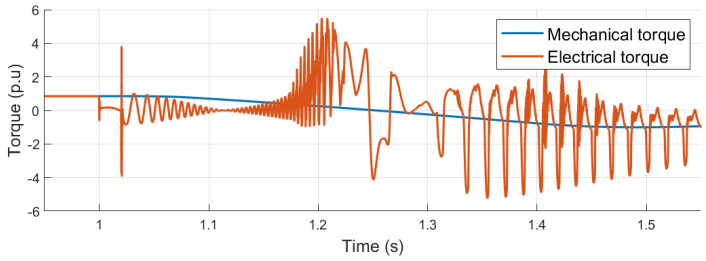

Fig. 10: Short circuit: machine torques

speed, as seen in Fig. 9d. After the short circuit clearance, the governor -that was trying to lower the machine's speed- is not providing the machine with enough mechanical torque to take on the upcoming electrical torque, that goes up after the short circuit's clearance. On top of that, the unstable current coming from the machine heavily distorts the local busbar voltage, making it harder for the governor to stabilize the rotor.

Conclusions

In this work, an implementation of the electrostatic machine model in a simulation software was achieved. Then, this machine was incorporated into a low voltage microgrid, along with a classical governor model and a modified AVR controller, in order to evaluate its operation as a generator. The results prove that this machine is able to participate in primary frequency control with a classical governor model, although with a slow response. In addition, the adapted ACR was able to keep the output power of the machine at a constant power factor. While this feature does not allow for direct participation in primary voltage control, it proved useful as a means of keeping the machine working in a certain operating condition.

The line disconnection experiment shows that, compared to a current source inverter, there is no need of re-tuning for the microgrid's protection scheme. This was expected, as the machine is modelled as a controlled current source; and given its inertia, fast variations are damped.

During the short circuit experiment, it was shown that the adapted controllers have a hard time dealing with such an event. This happens mainly due to the inability of the machine to provide torque, given the quick drop in the grid's voltage. This suggests that the machine might need a faster governor and a slower current controller, as a means to maintain synchronism.

Future work

This work's main goal was to explore the incipient development of electrostatic machines, and detect its possible contributions and challenges. As such, the experiments prompt for a lot of future research. First, the implemented controllers were not specifically designed for an electrostatic machine; they were slightly adapted. Therefore, there is a lot of room for improvement. As mentioned previously, and suggested by the experimental results, faster governors might have a significant impact on the machine's transient behavior, and a well designed ACR might let this machine participate in primary voltage control.

Machine dampers were not implemented in this machine's models. As of today, no physical implementation of these circuits has been published. Depending on their characteristics, these might have a great impact on the machine's behavior.

Finally, there is a lot of analytic work to be done in regards to this machine's operating conditions. Following the work in [4], power transfer equations can be extracted, and a capability curve can be obtained. These might give great insight on the machine's stable operating points and controller design.

References

[1] D. Gignoux, "Electrostatic generators in space power systems," AIAA 1964-450. 1st Annual Meeting, June 1964.

[2] F. J. McCoy and W. R. Bell, "Electrostatic generators for power production," Conference on Electrical Insulation & Dielectric Phenomena — Annual Report 1967, 1967, pp. 138-146.

[3] B. Ge and D. C. Ludois, "Dielectric liquids for enhanced field force in macro scale direct drive electrostatic actuators and rotating machinery," in IEEE Transactions on Dielectrics and Electrical Insulation, vol. 23, no. 4, pp. 1924-1934, August 2016.

[4] B. Ge, A. N. Ghule and D. C. Ludois, "High Torque Density Macro-scale Electrostatic Rotating Machines: Electrical Design, Generalized $d-q$ Framework, and Demonstration," in IEEE Transactions on Industry Applications, vol. 55, no. 2, pp. 1225-1238, March-April 2019.

[5] A. N. Ghule, P. Killeen and D. C. Ludois, "Synchronous Electrostatic Machine Torque Modulation via Complex Vector Voltage Control With a Current Source Inverter," in IEEE Journal of Emerging and Selected Topics in Power Electronics, vol. 8, no. 2, pp. 1850-1857, June 2020.

[6] A. Cuculić, D. Vučetić, R. Prenc, and J. Ćelić, "Analysis of Energy Storage Implementation on Dynamically Positioned Vessels," Energies, vol. 12, no. 3, p. 444, Jan. 2019.

[7] Papathanassiou, S., Hatziargyriou, N., & Strunz, K. "A benchmark low voltage microgrid network." In Proceedings of the CIGRE symposium: power systems with dispersed generation (pp. 1-8), CIGRE, April 2005.

[8] Diesel turbine datasheet, model n. P13.5-, 12.5 [kVA], by FGWilson™. (Online) Available: `https://www.fgwilsonpowerworks.com/brochures/uXQgbPAuCw.pdf/P13%205-6.pdf`, Visited on June 26, 2022.

[9] Exciter Models: Standard Dynamic Excitation Systems in NEPLAN Power System Analysis Tool. NEPLAN AG, Oberwachtstrasse 2, 8700 Küsnacht ZH, Switzerland. (Online) Available: `https://www.neplan.ch/wp-content/uploads/2015/08/Nep_EXCITERS1.pdf`. Visited on June 26, 2022.

[10] Turbine Governor Models: Standard Dynamic Turbine-Governor Systems in NEPLAN Power System Analysis Tool. NEPLAN AG, Oberwachtstrasse 2, 8700 Küsnacht ZH, Switzerland. Available (Online): `https://www.neplan.ch/wp-content/uploads/2015/08/Nep_TURBINES_GOV.pdf` Visited on June 26, 2022.